ACS Photonics

pubs.acs.org/journal/apchd5

Perspective

Photonic Assemblies of Randomly Oriented Nanocrystals for Engineered Nonlinear and Electro-Optic Effects

Viola Valentina Vogler-Neuling,[†] Artemios Karvounis,*[,†] Andrea Morandi, Helena Weigand, Eric Dénervaud, and Rachel Grange

Cite This: *ACS Photonics* 2022, 9, 2193−2203

Read Online

ACCESS | Metrics & More | Article Recommendations

ABSTRACT: Nonlinear crystals that have a noncentrosymmetric crystalline structure, such as lithium niobate ($LiNbO_3$) and barium titanate ($BaTiO_3$) exhibit nonzero second-order tensor susceptibilities ($\chi^{(2)}$) and linear electro-optic coefficients (r_{ij}). The constraints associated with top-down nanofabrication methods have led to bottom up approaches to harness the strong nonlinearities and electro-optical properties. Here, we present an overview of photonic assemblies made of randomly oriented noncentrosymmetric nanocrystals via bottom-up fabrication methods. In this configuration, nanocrystals can form objects with tunable dimensions, increased complexity, and a great span of symmetry level, ranging from thin layers to spheres. At the same time, according to their shape, photonic assemblies may support optical modes, that is, Mie or guided, which can tailor linear optical properties and enhance nonlinear and electro-optic responses. As a result, assemblies of noncentrosymmetric nanocrystals can form a disruptive platform to realize photonic integrated devices free of etching process and over large surface areas. Last, we foresee potential applications of noncentrosymmetric nanocrystals in various fields of nano-optics and sensing.

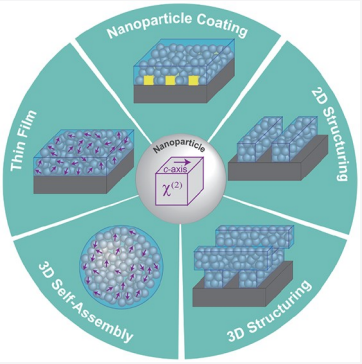

KEYWORDS: *nanoparticles, barium titanate, lithium niobate, second harmonic generation, bottom-up, assemblies*

INTRODUCTION

Among the class of nonlinear materials, there are crystals that exhibit second-order nonlinearities and the linear electro-optic effect due to the lack of an inversion symmetry center (noncentrosymmetric) in their crystal structure. These materials are used in numerous daily life applications, ranging from light sources for microsurgery and green laser pointers, up to optical metrology and modulators for telecommunication networks.[1] However, these devices utilize high-quality bulk crystals that are neither integrable due to limited compatibility with top-down nanofabrication methods compared to typical semiconductors, nor scalable due to the low generated signals, especially in frequency conversion on a small scale. Therefore, enabling methods to harvest their functional response at the nanoscale will favor energy requirements and simplify their fabrication. However, scaling down the dimensions of noncentrosymmetric crystals can meet various physical constraints related to the phase matching conditions between interacting fields, as well as reduced electro-optic coefficients compared to bulk crystals. Recent advances based on photonic assemblies of randomly oriented nanocrystals instead of bulk crystals, have produced nonlinear optical signals with excellent properties related to frequency doubling and electro-optic response at the nanoscale.[2] At the same time, these new material candidates have to facilitate fabrication protocols compared to standard semiconductors in order to expand their applications toward photonic integrated devices (PICs).

Besides the booming of lithium niobate on insulator (LNOI), thanks to the availability of thin film substrate of this oxide,[3] with tremendous effort in the top-down fabrication,[4] there is also the bottom-up development of noncentrosymmetric metal oxides. Indeed, nanocrystals and sol−gels of metal oxides, such as lithium niobate ($LiNbO_3$) and barium titanate ($BaTiO_3$), normally used as bulk, are promising alternatives to high-quality crystals. Here, we give an overview and the potential application of photonic assemblies based on noncentrosymmetric nanocrystals.

In the early 2000, nonlinear optical effects, such as second-harmonic generation (SHG) or third-harmonic generation (THG) were produced by several types of nanoparticles. For example, potassium titanyl phosphate (KTP)[5] and zinc oxide (ZnO),[6] produced either by grinding or synthesizing them, have been used for nonlinear frequency conversion on a very small scale. This field of second-harmonic probes remains very

Received: January 17, 2022
Revised: June 17, 2022
Accepted: June 21, 2022
Published: July 6, 2022

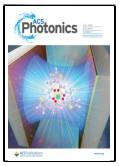

https://doi.org/10.1021/acsphotonics.2c00081
ACS Photonics 2022, 9, 2193−2203

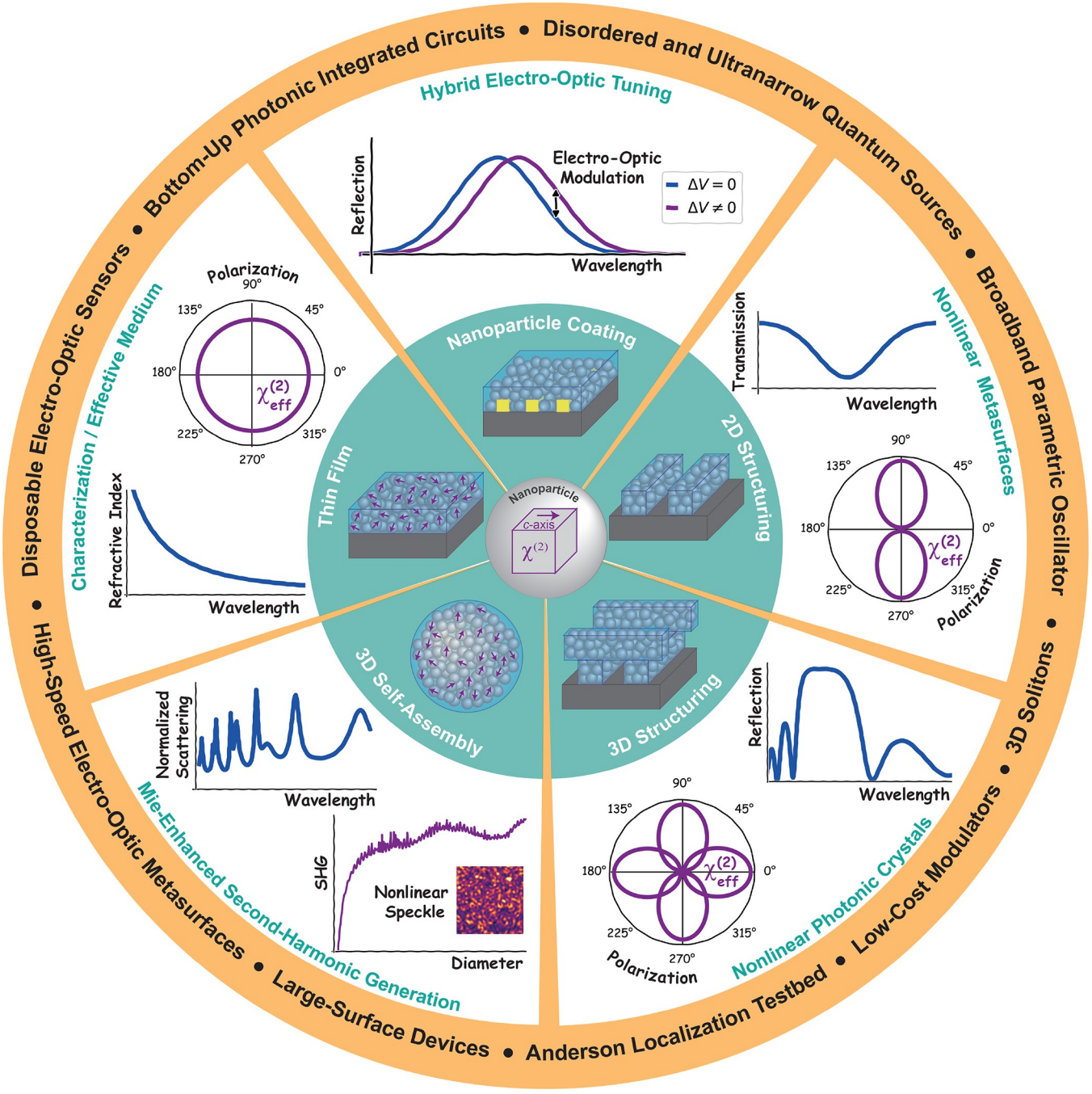

Figure 1. Photonic assemblies of noncentrosymmetric nanocrystals for engineering nonlinear and electro-optic effects. Nanoparticles are composed out of a crystallite core, named nanocrystal (purple surrounded cube), which is responsible for the nonlinear responses and an amorphous shell (gray). These nanoparticles can be assembled by different techniques in versatile geometries such as thin films, planar structures, e.g., metasurfaces, or even three-dimensional stuctures such as photonic crystals and microspheres. The random orientation of the *c*-axis direction of every nanocrystal (purple arrow) leads to an effective nonlinear response of the photonic assembly. The randomly oriented nanoparticles can be combined with hybrid platforms such as plasmonic metasurfaces or be brought into different shapes in two and three dimensions (turquoise areas). Such structures modify or even enhance the electro-optic, as well as the nonlinear optical responses of the individual nanoparticles (white areas). The different platforms can lead to applications (orange areas) as disposable electro-optic sensors, disordered quantum sources, or generate 3D solitons.

active for the multiphoton bioimaging capabilities of the nanoparticles[7] and its application in nanomedicine.[8] Moreover, the incorporation of noncentrosymmetric nanocrystals of subwavelength size with noble metals can engineer nonlinear responses further due to the excitation of plasmonic or Mie resonances.[9,10]

There are studies where the crystal structure of $LiNbO_3$ nanoparticles is preserved down to diameters as small as 5−50 nm,[11] while individual $BaTiO_3$ nanoparticles maintain their bulk behavior and generate second-order signals down to 30 to 40 nm in diameter.[12] Moreover, it has been shown for larger sizes of particles (e.g., 300−400 nm in diameter) that the crystalline structure relaxes from tetragonal in the core to cubic at the surface. This was probed with nonlinear imaging[13] and confirmed with Raman spectroscopy.[14] But what remained unexplored until recently is the behavior of these nanocrystals

https://doi.org/10.1021/acsphotonics.2c00081
ACS Photonics 2022, 9, 2193−2203

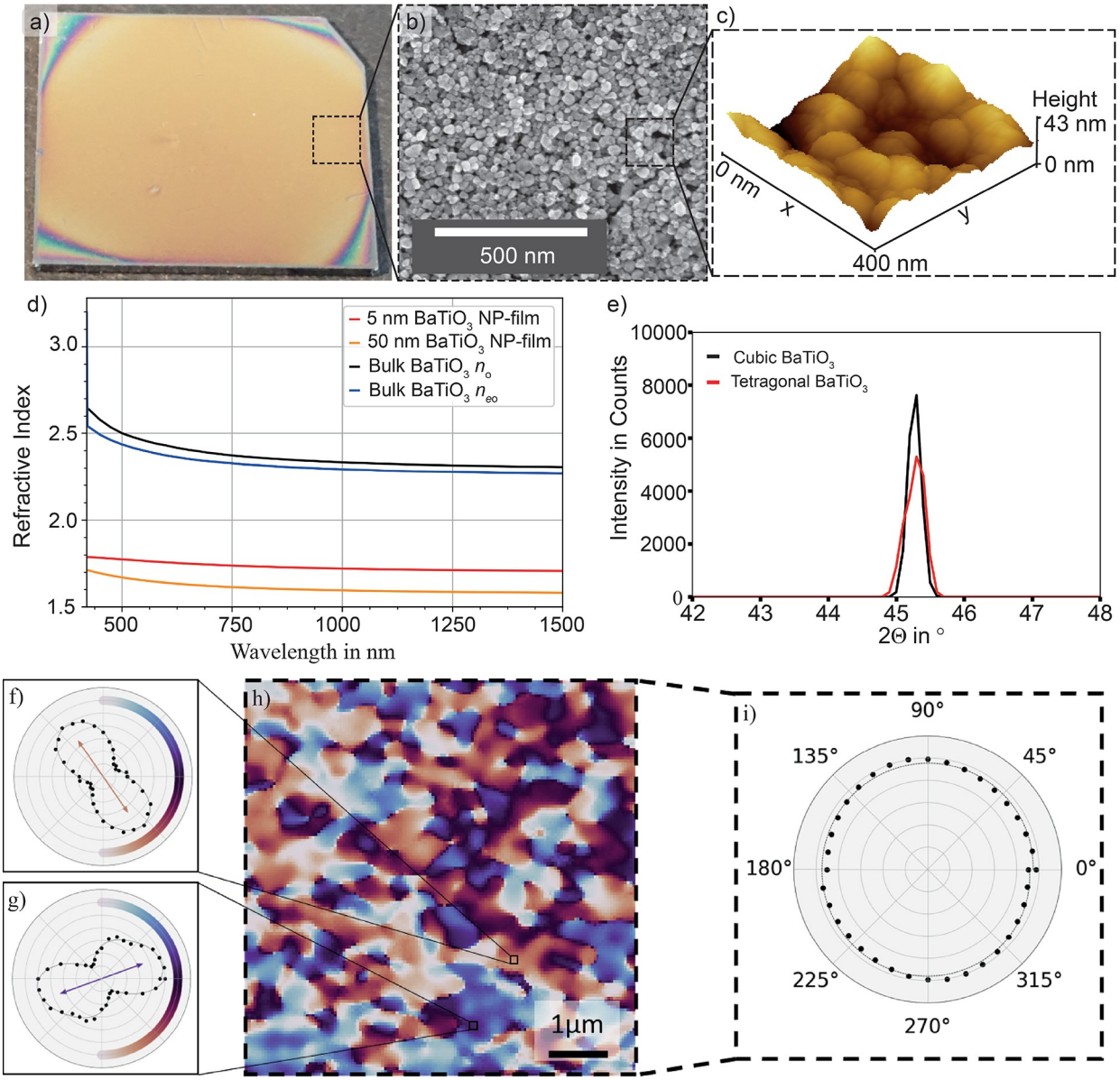

Figure 2. (a) Optical image of a 1.5 × 1.5 cm^2 large $BaTiO_3$ nanoparticle thin film deposited on silicon with a thickness of 246 nm. (b) High magnification SEM image of a nanoparticle thin film deposited as in (a). (c) Atomic force microscopy image showing the surface roughness of the nanoparticle thin film. (d) Refractive index of nanoparticle films prepared of 5 and 50 nm sized $BaTiO_3$ nanoparticles compared to the bulk ordinary (n_o) and extraordinary (n_{eo}) refractive index values of $BaTiO_3$. (e) X-ray diffraction pattern at the peak of 45.3° for a $BaTiO_3$ nanoparticle film; with a cubic and tetragonal fitting. (f–i) Second-harmonic generation measurements on a thin film of $BaTiO_3$ nanoparticles with diameters of approximately 50 nm. (h) Different domains on the thin film have different orientation and shape of the SHG polarization response (f) and (g). (i) Integrating over the whole surface area, results in a circular polar dependence which demonstrates the random orientation of the nanocrystals.

upon the formation of assemblies. Are their SHG signals randomly interfering and becoming destructive? What happens if an electric field is applied? Is the linear electro-optic effect present in nanoparticle assemblies? Recent advancements answer these questions and present applications of assembled nanocrystals toward photonic integrated devices in sensing and nano-optics. Over the past years, the research over non-centrosymmetric nanocrystals that started with single particles has expanded to complex assemblies.

The family of various photonic assemblies made from $BaTiO_3$ nanocrystals is schematically shown in Figure 1. From the nanoparticle building block (center of Figure 1) to thin films, planar and three-dimensional structures (turquoise areas of Figure 1) are realized via bottom-up fabrication. Their typical photonic responses are presented in the white areas of Figure 1, and some potential applications are mentioned in the surrounding orange crown.

In this Perspective we present the second-order nonlinear susceptibility ($\chi^{(2)}$) and the linear electro-optic coefficients (r_{ij}) expressed in the tensorial form of bulk $BaTiO_3$. Next, we report recent methods to produce thin films of randomly oriented nanocrystals and the respective characterization techniques. Then, we present how planar and three-dimensional structures made by bottom-up fabrication are utilized to deliver resonant nanostructures such as photonic metasurfaces, photonic crystals, and Mie-resonant microspheres. We restrict the discussion in the article to the material platform of barium titanate. However, the methods and applications can be

https://doi.org/10.1021/acsphotonics.2c00081
ACS Photonics 2022, 9, 2193−2203

applied to most nanocrystals with a noncentrosymmetric crystal structure. Last, we foresee possible future directions with this material platform.

NONCENTROSYMMETRIC CRYSTALS FROM BULK TO NANOSTRUCTURES

The lack of inversion symmetry of the crystal structure macroscopically manifests as the spontaneous polarization of the crystal, and it is generally controlled with the electrical poling of the crystal. Microscopically, it can be understood as the contribution to the net dipole moment from every individual unit cell of the crystal. Within a single unit cell there are several possible orientations of the dipole moment in respect to the crystallographic axis. Neighboring atoms that possess the same direction of the dipole moment form a domain. For example, in the tetragonal phase of $BaTiO_3$, the direction of the dipole moment is aligned with the *c*-axis, while the other two orthogonal directions are called *a*-axes. This difference is also translated in different refractive indices for light polarized along the *c*- or *a*-axis, named extraordinary (n_{eo}) and ordinary refractive indexes (n_o), respectively. A mathematical tensor is used to describe the second-order susceptibilities and electro-optic coefficients for each type of noncentrosymmetric crystal for a given phase. Specifically, at room temperature, $LiNbO_3$ has a trigonal crystal structure, while $BaTiO_3$ has a tetragonal crystal structure. The characterization of these parameters is of paramount importance, as light propagating over a specific crystallographic axis will experience direction-dependent second-order nonlinearities and electro-optic responses. The second-order polarization vector $P^{(2)}$ is given by eq 1:

$$P_i^{(2)} = \sum_{j,k} \epsilon_0 \chi_{ijk}^{(2)} E_j E_k \tag{1}$$

where the tensor $\chi_{ijk}^{(2)}$ is a third rank tensor consisting of 27 components, and the E_j and E_k are components of the driving electric field vector. The second-order susceptibility $\chi^{(2)}$ of $BaTiO_3$ is reduced to a matrix, named reduced tensor, which has three independent components:

$$d_{BTO} = \begin{pmatrix} 0 & 0 & 0 & 0 & d_{15} & 0 \\ 0 & 0 & d_{15} & 0 & 0 & 0 \\ d_{31} & d_{31} & d_{33} & 0 & 0 & 0 \end{pmatrix}$$

where $P^{(2)} = 2\epsilon_0 dE^2$ and $E^2 = [E_x^2 E_y^2 E_z^2\ 2E_yE_z\ 2E_xE_z\ 2E_xE_y]^T$ a more detailed description of the tensor components can be found in Sutherland et al.[15]

The electro-optic response of $BaTiO_3$ is described by the following tensor:

$$r_{BTO} = \begin{pmatrix} 0 & 0 & r_{13} \\ 0 & 0 & r_{23} \\ 0 & 0 & r_{33} \\ 0 & r_{42} & 0 \\ r_{51} & 0 & 0 \\ 0 & 0 & 0 \end{pmatrix}$$

according to the annotation of Zgonik et al.[16]

The maximum values for bulk $BaTiO_3$ are $d_{15} = 17\ pm\ V^{-1}$ and $r_{42} = 730\ pm\ V^{-1}$. In a similar way, the maximum values of bulk $LiNbO_3$ are $d_{33} = -27\ pm\ V^{-1}$ and $r_{51} = 32\ pm\ V^{-1}$,[17] for near-infrared light. How are these values affected for individual nanoparticles or more complex assemblies? Special characterization techniques can address whether the developed assemblies maintain their nonlinear response.

THIN FILMS OF RANDOMLY ORIENTED NANOCRYSTALS

$LiNbO_3$ thin film crystals fabricated by crystal ion slicing and wafer bonding, produce relatively uniform and single domain films.[3] $BaTiO_3$ thin films have been successfully produced by high vacuum systems such as molecular beam epitaxy (MBE) or pulsed laser deposition (PLD).[18,19] These techniques create a homogeneous film with multiple oriented domains. Alternatively, $BaTiO_3$ nanocrystal thin films can also be produced by close packing of individual nanoparticles (Figure 2a−c), where each nanoparticle contains a single nanocrystal.[20,21] Here, we focus our discussion on thin films prepared by $BaTiO_3$ nanoparticles but the concept can be transferred to other nanocrystals as well.

The reason why crystallites are required inside the nanoparticles, is that nonlinear optical properties such as second-harmonic generation or the electro-optic effect rely on an intact crystalline structure. Therefore, the material cannot be in an amorphous state, but it has to be as polycrystalline as possible. Monocrystalline samples are expected to demonstrate responses similar to bulk, however, these are not possible to fabricate, even with the most sophisticated deposition methods, as MBE.[19]

Thin films prepared from nanoparticles (Figures 2a,b) form an effective medium among the crystallite, the amorphous shell surrounding the crystallite, and the surrounding material, which can be either air or some other filling material. Compared to the bulk values, the refractive indices of the effective medium is reduced.[2] Figure 2d presents the refractive index over visible and near-infrared wavelengths of bulk barium titanate ($n \sim 2.3$) and nanoparticle thin films composed of 5 nm sized solvo-thermally grown nanoparticles ($n \sim 1.7$)[22] and 50 nm sized hydrothermally grown nanoparticles ($n \sim 1.6$).[20] The measurement of the refractive index of the composite films requires to take into consideration the nonzero surface roughness (Figure 2c); therefore, fitting models used in ellipsometry are inaccurate due to the effective medium structure. However, the prism-coupling technique is adequate for the refractive index analysis of such composite films.[23] The production of higher refractive index nanoparticle films is necessary in order to enhance the mode confinement inside the photonic structures. There are different strategies on how to achieve this. From Figure 2d, it stems that smaller nanoparticle diameters result in higher refractive indices; however, there is an experimental and theoretical limit down to which diameter of $BaTiO_3$ is still in the noncentrosymmetric tetragonal phase.[12] Another approach is to embed the nanoparticles inside a high index filling material. As photonic nanocrystals are reduced in size, we cannot anymore assume that second-order susceptibilities and electro-optic coefficients will be equal with the bulk counterparts. For $BaTiO_3$, the bulk r_{42} component yields $730\ pm\ V^{-1}$,[16] thin films produced by MBE yield effective electro-optic coefficient in the range of 140 up to $200\ pm\ V^{-1}$[24,25] and a sol−gel-derived barium titanate yields $27\ pm\ V^{-1}$[26], which is still on the order of the electro-optic coefficient of bulk $LiNbO_3$ ($r_{15} = 32\ pm\ V^{-1}$).[27]

https://doi.org/10.1021/acsphotonics.2c00081
ACS Photonics 2022, 9, 2193−2203

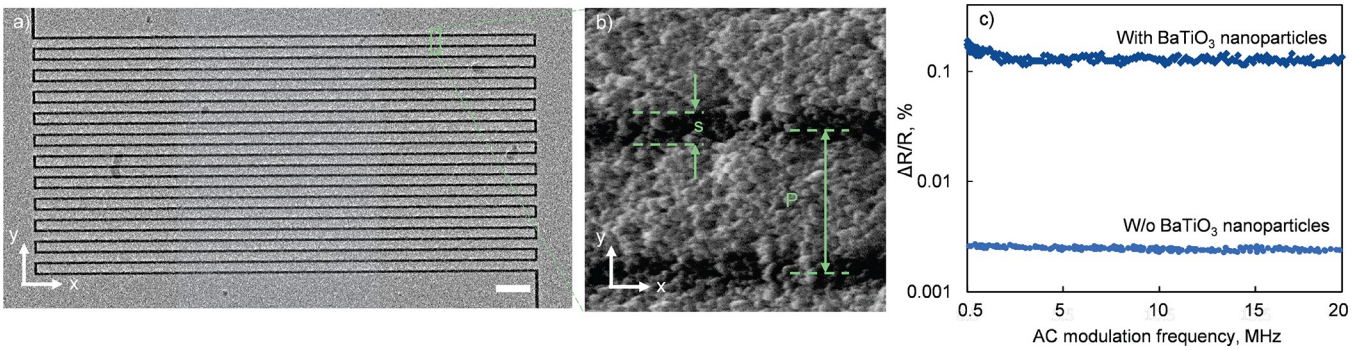

Figure 3. Electro-optic metasurface based on $BaTiO_3$ nanocrystals. (a) SEM image of a periodic array of gold (Au) nanowires coated with $BaTiO_3$ nanocrystal film (scale bar 2 μm). (b) Magnified cross-sectional SEM image of the metasurface, period and slit size are annotated by P = 600 nm and s = 150 nm, respectively. (c) Relative reflectivity change, ΔR of the optical signal for the metasurface with and without nanoparticles, as a function of the AC modulation frequency. Adapted with permission from ref 21. Copyright 2020 Wiley-VCH; https://creativecommons.org/licenses/by/4.0.

CHARACTERIZATION OF RANDOMLY ORIENTED NANOCRYSTALS

The characterization of the crystalline structure is crucial to develop high performing nonlinear optical devices, in terms of SHG and electro-optic response. $BaTiO_3$ exhibits peaks in the X-ray diffraction (XRD) pattern at 2θ = 45.3°, 50.9°, 56.2°, and 65.8°. The ratio between the c- and the a-axis of bulk tetragonal barium titanate is c/a = 1.01.[28] The peak to distinguish the tetragonal from the cubic phase is the peak at 45.3° corresponding to the (002) plane (Figure 2c). This peak splits up for the tetragonal phase into two distinct peaks (002) and (200). By scaling the material down to the nanometer scale, XRD cannot probe the crystal structure as there are not enough planes left to produce complete destructive interference due to the smaller crystallite sizes (Figure 2e). Therefore, XRD is suited to prove that the engineered material is indeed $BaTiO_3$ and it can give an indication whether the material is tetragonal or cubic but a quantification is not possible. Raman spectroscopy is an additional characterization method to distinguish the tetragonal from the cubic phase. The peak at 306 cm^{-1} is the essential peak to look at, as it does not persist into the cubic phase, but this peak is also dependent on the grain size, as it shifts to longer inverse wavenumbers for smaller grain sizes.[14] Furthermore, the relative intensity of this peak is reduced if the tetragonal phase is mixed with the cubic or amorphous phase. If this is up to date is still an open question. A more powerful technique to probe the noncentrosymmetric structure is optical second-harmonic spectroscopy.

As the SHG process is forbidden in bulk centrosymmetric materials, this technique allows differentiating the SHG active tetragonal phase from the non-SHG active cubic phase of $BaTiO_3$. The sensitivity of the SHG signal intensity to the polarization state of the fundamental beam probes both the crystal structure and the orientation of the c-axis. Figure 2f–i show a polarization-dependent SHG measurement done on a spin-coated $BaTiO_3$ nanoparticle thin film. The measurement was done with a homemade setup described elsewhere.[29] The color scale of the SHG polar map in Figure 2f–h is directly related to the orientation of the SHG anisotropy pattern. In each pixel, a statistical approach is performed to compute the principal component (axis) of the polar anisotropy represented by the arrow on the polar plots. The orientation of the principal axis, defined with angles from 0° to 180°, is used to color the pixel, as shown with the color scale on the right side of the anisotropy. The tetragonality of the film is first verified as the SHG signal is produced at any position in the 7 μm × 7 μm region of interest. In addition to that, the SHG polar map in Figure 2f shows distributed domains with different SHG anisotropy patterns that are larger in size than the individual nanoparticle diameters. The pixel-by-pixel analysis of the SHG signal enables one to get information about the crystal structure locally with a high spatial resolution. In Figure 2f,g, two polar plots integrated over a small region (approximately 80 nm × 80 nm) are presented, which show sharp polar dependencies with different orientations. However, the integration of the SHG signal over the full region of interest, (shown in Figure 2h) results in a circular polar plot (Figure 2i) originating from the random c-axis orientation of the nanoparticles over such a large area. It would be desirable in the future to have one characterization method that can provide the researcher with an exact number of the tetragonality in noncentrosymmetric nanocrystal thin films to improve the engineering of the optical performance. To boost the nonlinear performance of noncentrosymmetric nanocrystal thin films postannealing or deposition on lattice-matched substrates can be applied.[30,31] In comparison to nonlinear thin films produced by smart cut technologies (e.g., lithium niobate), polycrystalline nonlinear films are produced with reduced fabrication complexity and retain comparable electro-optic coefficients.[26,27] The randomly oriented thin films can be combined with nanostructures of other materials, for example, noble metals, or they can be structured directly in different nanostructure geometries. The overall goal is to enhance the electro-optic, as well as the second-harmonic properties by exploiting optical resonances to increase the refractive index change or the frequency conversion efficiency.[32]

ELECTRO-OPTIC PHOTONIC METASURFACES

As we presented before, noncentrosymmetric crystals apart from the second-order optical nonlinearity support the linear electro-optic or Pockels effect. There is a link between the linear electro-optic coefficient and the reduced second-order susceptibility coefficients, which is described by Kleinman et al., and it is calculated to be $r_{ij} = -4\pi A_j d_{ij}$, where A_j is the element of the principal inverse dielectric constant of the bulk crystal.[33] The advantage of the linear electro-optic effect over any other electro-optic mechanism is the ultrafast response. Therefore, continuous research is being made on the development of thin devices (submicron thickness) based on

https://doi.org/10.1021/acsphotonics.2c00081
ACS Photonics 2022, 9, 2193–2203

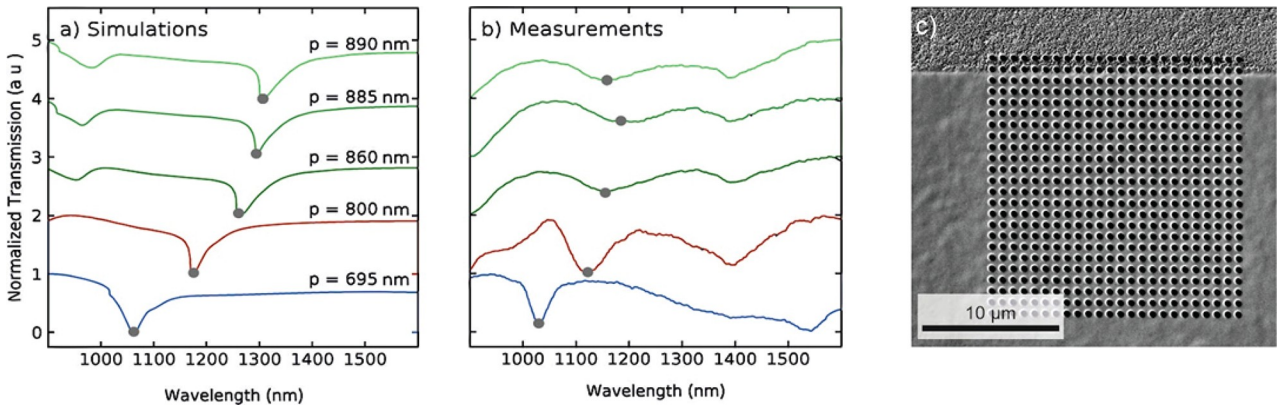

Figure 4. $BaTiO_3$ metasurface made from $BaTiO_3$ nanocrystals via FIB. (a) Simulation of the resonant behavior in transmission for various metasurface periods (p). (b) Normalized transmission measurements on fabricated sample. The curves in (a) and (b) have been shifted by a constant offset for better readability. (c) SEM image of fabricated structure with smoothened surface. Reproduced with permission from ref 43. Copyright 2020 The Optical Society.

these materials. This effort has allowed the scale-down of bulk crystals into compact electro-optic thin films that could form waveguides and several other types of nanostructures.[34−36] $LiNbO_3$ in the bulk and in the thin film form, subject to electrical poling, can align the net polarization over large domains permanently. In the case of $BaTiO_3$ thin films, electrical biasing is more complex, as $BaTiO_3$ thin films tend to form nanodomains that can be flipped along the preferred directions either in reversible or irreversible fashion. Still, there is a trade-off between the fabrication cost and the quality of the thin films produced. However, thin films of randomly oriented nanocrystals are produced by close packing of individual nanoparticles, offering a disruptive method to realize films of high electro-optic coefficient with low fabrication cost and compatibility with any type of substrate. We recently reported that plasmonic metasurfaces coated by thin films of $BaTiO_3$ nanoparticles can have electro-optic response larger than commercial $LiNbO_3$-based electro-optic modulators that can reach a response speed up to 95 MHz.[21,37]

Photonic systems related to plasmonic metals and metasurfaces have enabled the manipulation of light at the subwavelength scale. They have been employed successfully in planar nanocircuit designs based on either surface or localized plasmon polaritons to realize devices with application among others in nonlinear optics,[38] ultrafast active plasmonics,[39] and electro-optic modulators.[40] In the latter case, the spatial overlap between the optical mode and the electric field provides a platform of greatly enhanced electro-optical coupling. We believe that optically resonant nanostructures and particularly plasmonic metasurfaces can offer a playground to engineer the electro-optic coupling, as well as, to reduce the device power consumption, due to the small seperation distance (submicron scale) of the actuation electrodes.

Figure 3 presents a SEM image of such an electro-optic metasurface based on $BaTiO_3$ nanocrystals. The electro-optic metasurfaces are composed of a subwavelength plasmonic nanograting coated by a thin film of $BaTiO_3$ nanoparticles. The overall thickness of the samples were smaller than 300 nm, resulting in subwavelength interaction lengths. The $BaTiO_3$ films were produced by drop casting a solution of water with 25 wt % of $BaTiO_3$ nanocrystals and subsequent spin-coating at 3000 rev min^{-1} to produce a thin coating of 200 nm. Average diameter of the nanocrystals is 50 nm. The metasurface response was tested at the wavelength of 1064 nm and in reflection mode. The electro-optic response speed was tested up to 20 MHz and the effective EO coefficient of the nanocrystal film estimated to be around 40 pm V^{-1}. Further investigation of domain formation in such complex films may be realized via SHG measurements mentioned in previous paragraph or similar to methods reported by Nordlander et al.[41]

The actuation voltage is comparable to the films produced by MBE methods, while the electro-optic coefficient is an order of magnitude smaller. Moreover, nanoparticle films can be coated on any type of substrate overcoming substrate limitation on deposition methods as PLD and MBE, where lattice-matched substrates are required.

ALL-NANOPARTICLE PHOTONIC METASURFACES

Photonic devices from noncentrosymmetric nanocrystals cannot only be realized as hybrid plasmonic−dielectric structures, but can also be constructed as purely dielectric devices. This approach was already shown in linear media such as titanium dioxide (TiO_2)[42] and only recently with noncentrosymmetric nanocrystals. These metasurfaces are realized as periodic arrangements of subwavelength circular holes in a $BaTiO_3$ nanoparticle film.[43] Simulations based on finite element methods show a dielectric resonance in the near-infrared. Transmission spectra indicate that the spectral position of the resonance is controlled by the period of the unit cell (Figure 4a,b). The sample was fabricated by direct focused ion beam milling (FIB) on a previously spin-coated $BaTiO_3$ nanoparticle film on a quartz substrate. After the metasurface fabrication, a FIB raster scan over the samples reduced roughness of the films in order to minimize optical losses associated with scattering displayed in Figure 4c, where the contrast between the grainy and the smooth surface is clearly visible. The acceleration voltage and beam current were kept at values low enough to avoid additional optical losses, namely, at 8 keV and 7 pA. The transparent substrate allowed transmission measurements in the visible to near-infrared range, where the authors confirmed the influence of the periodicity on the optical transmission (Figure 4b). Further optimization of the metasurface design and the incorporation with fabrication methods, such as roll-to-roll techniques or soft-nanoimprint lithography, would allow the high-throughput

https://doi.org/10.1021/acsphotonics.2c00081
ACS Photonics 2022, 9, 2193−2203

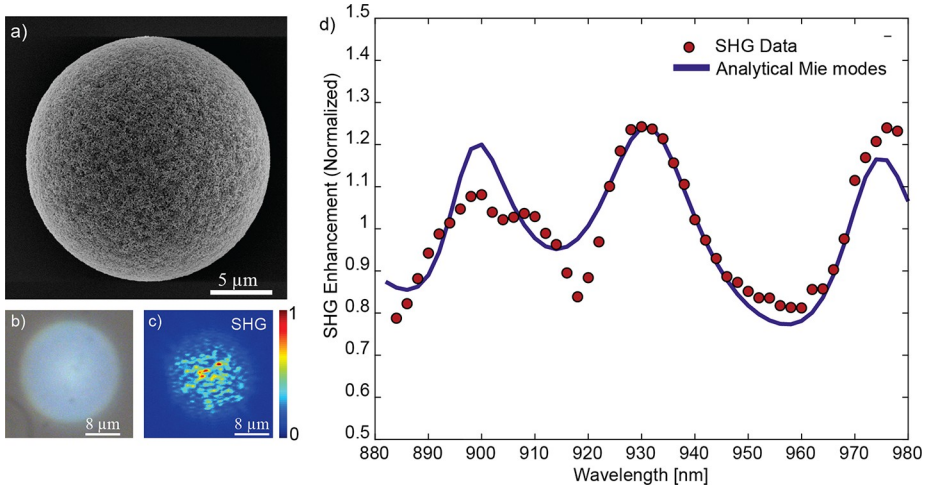

Figure 5. Second harmonic generation from an assembled $BaTiO_3$ microsphere. (a) SEM image of a microsphere assembled by individual $BaTiO_3$ nanoparticles of average size of 50 nm. (b) Bright-field optical image, the light blue color stems from the weak Rayleigh scattering. (c) Spatial distribution of the SHG emitted from a $BaTiO_3$ microsphere. The red and blue spots (speckle pattern) are the result of the interference of light generated in each of the randomly oriented nanocrystal. (d) SHG of a microsphere of diameter 2.5 μm obtained by sweeping the pump wavelength from 880 to 980 nm. The modes in the data are fitted with an analytical model obtained by Mie theory and effective medium calculation. Adapted with permission from ref 45. Copyright 2020 Springer Nature Ltd.

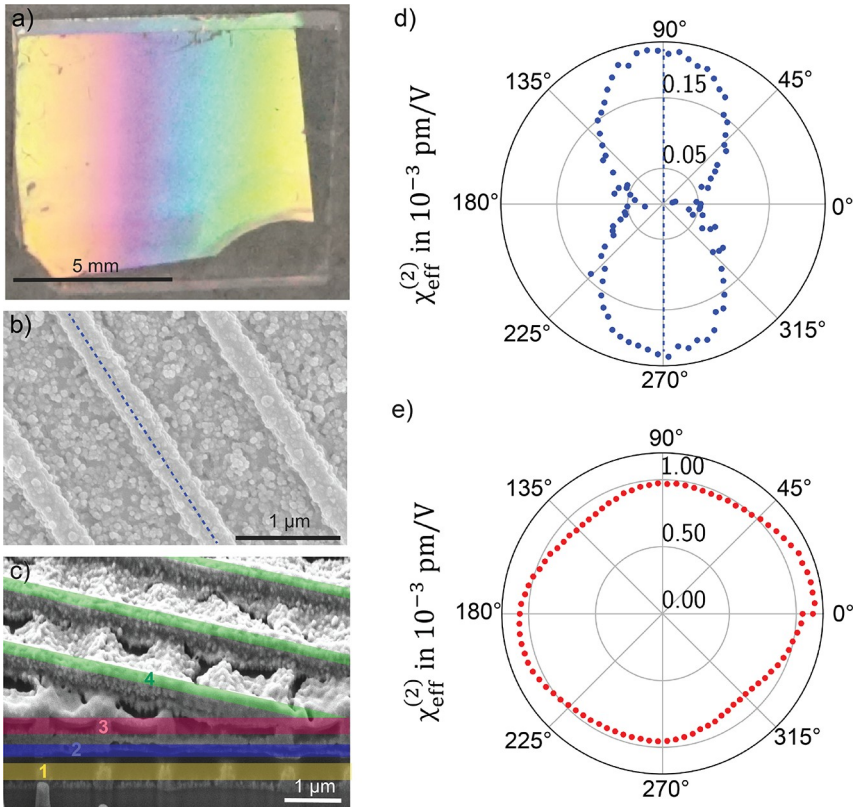

Figure 6. Imprinted $BaTiO_3$ grating and woodpile. (a) Optical image showing an imprinted grating over large surface area of 1.0 cm^2. (b) SEM image of a grating with 1 μm pitch, 506 nm width, and a height of 260 nm. The blue dotted line is indicating the direction of the long axis of the nonlinear dipole response from the structure. (c) A cross-sectional SEM image of a four-layer woodpile photonic crystal. The numbers 1 (yellow) to 4 (green) annotate each layer, false color is used for better visibility. (d) Second-harmonic polarization response of grating for a pump wavelength of 1000 nm. The long axis of the dipole (blue dotted line) is parallel to the rod orientation depicted in (b). (e) Second-harmonic polarization response of an eight-layer woodpile photonic crystal for a pump wavelength of 800 nm. The dipoles from each individual layer are adding up and yielding in a quadrupole response. Adapted with permission from ref 20. Copyright 2020 Wiley-VCH; https://creativecommons.org/licenses/by/4.0.

and cost-effective fabrication of assemblies of noncentrosymmetric nanocrystals.[44]

https://doi.org/10.1021/acsphotonics.2c00081
ACS Photonics 2022, 9, 2193−2203

THREE-DIMENSIONAL PHOTONIC ASSEMBLIES OF RANDOMLY ORIENTED NANOCRYSTALS

Photonic assemblies of nanocrystals can also be constructed with different bottom-up techniques in two- or three-dimensional photonic structures. The resulting disordered assemblies are constituted by a polydisperse and randomly arranged distribution of noncentrosymmetric crystalline domains. For such a disordered medium it is impossible to define a global $\chi^{(2)}$, while locally the nonlinear tensor is well-defined by the nanocrystals. When these nonlinear and disordered assemblies are driven by an optical pump beam, each of the constituting nanocrystals generates second-harmonic proportional to the square of its volume. Counter-intuitively, the interference of the SHG generated from the crystalline domains is not destructive but instead scales linearly with the volume of the whole assembly.

This nonlinear mixing regime is called random quasi-phase-matching (RQPM).[45,46] The biggest advantage of this regime lies in the relaxed phase matching conditions, which enables the broadband nonlinear generation. RQPM has been exploited so far to realize disordered based optical-parametric-oscillators.[47] This regime is very robust, and it is still valid in media with light scattering, where the nanocrystals have size comparable to the wavelength. In fact, nonlinear light emitted from assemblies of scattering nanoparticles can be a unique tool to investigate Anderson localization.[48] While the disorder in the $\chi^{(2)}$ is key to this process, it is possible to modify the global geometry of the assembly to shape the emission. It has been shown by Savo et al. that resonances in the disordered assembly can be exploited to boost the emission. In Figure 5a well-shaped microsphere is presented made of assembled $BaTiO_3$ nanocrystals and used to enhance the SHG, thanks to the coupling with Mie modes (Figure 5b,c).[49] This proved the coexistence of broadband emission, enabled by the random quasi-phase-matching, and modes in the assembly.

The randomly oriented nanocrystals can not only be self-assembled in three-dimensions, but they can also be templated in the form of three-dimensional nonlinear photonic crystals by soft-nanoimprint lithography. 3D photonic crystals with spatial periodicity over the $\chi^{(2)}$ susceptibility provide a platform to realize multidimensional entanglement, nonlinear multiplexing, and THz waves and also provide a scheme for fundamental atomic, molecular, and optical physics.[50] Due to the challenges in nanofabrication of noncentrosymmetric materials, so far only small surface areas (μm^2) and a low number of layers of 3D nonlinear photonic crystals have been achieved.[51] Photonic nanocrystals can allow for large surface areas (cm^2) and a larger amount of layers, which are not achievable with top-down fabrication approaches (Figure 6a−c).[20] These solution-processed $BaTiO_3$ nanocrystals combined with soft-nanoimprint lithography have proven to be able to modify the polar dependency of the random quasi-phase-matched SHG. In particular, it has been shown that a single layer of patterned $BaTiO_3$ produces a dipolar response of the SHG (Figure 6d). For the woodpile photonic crystal structure, up to four layers (one unit cell) have been stacked perpendicular on top of each other. These lead to a quadrupolar response from the whole system and provide a technique to demonstrate the $\chi^{(2)}$ periodicity of the structure (Figure 6e).

PERSPECTIVES

Assembled nanocrystals represent a versatile platform to realize electro-optic metasurfaces and broadband light sources, as long as the noncentrosymmetric crystalline structure is maintained at small dimensions. Quantifying their crystallinity, even in randomly oriented nanoparticle assemblies, is essential for photonic applications. We pointed out the main techniques (XRD, Raman, and SHG spectroscopy) in use now and their limitations to quantify the crystallinity, which is crucial to develop functional devices. We anticipate in the coming years that the accuracy of the characterization may be improved by new techniques. Furthermore, any discovery on the material side would be highly valuable for the applications. In particular, nanocrystals of smaller sizes that maintain the tetragonal phase could form assemblies of higher uniformity and result in improved optical resonant modes. A higher refractive index from the nanocrystal or its surrounding, for instance, by combining nanoparticles with a high-index polymer, is a key property for the strong confinement of light in the structure. Last but not least, the search over chemical recipes for the surface functionalization and the compatibility of nanocrystals with various substrates and complex structures could lead to devices with advanced performance.

We have provided evidence that photonic assemblies can be successfully coupled with optical resonances to produce functional devices without relying on phase matching conditions. Coupling a film of nanocrystals with a plasmonic metasurface can produce flat electro-optic modulators, with a bandwidth of 95 MHz, but this is not the limit; indeed, bulk lithium niobate can reach 100 GHz, and $BaTiO_3$ will do as well.[17,34,35] So, nanocrystals have a role to play in high-speed integrated photonics in the future. More specifically, assemblies of nanocrystals could form a thin layer on top of integrated plasmonic waveguides, similar to electro-active polymers.[52] Additionally, the incorporation of nanocrystals with optical polymers could result in a plethora of optical waveguides.[53] Moreover, we have presented assemblies of randomly oriented nanocrystals that do not rely on typical phase-matching conditions and allow for broadband SHG via random-quasi-phase-matching.[49] Their emission can be shaped by geometry, for example, tuning the polarization of the emission by structuring the $BaTiO_3$ film, and the design of any structures is possible by nanoimprinting or FIB. On top of that, the emission can also be enhanced by resonances similar to what happens in the microspheres, which the broadband emission is driven by Mie modes imposed by the outer geometry. The microspheres could be used as building blocks for producing broadband optical parametric oscillators following random quasi-phase-matching and with several resonances over a few hundred nanometers. For instance, a close packing of microspheres can be used as nonlinear and disorderd optical material to fabricate a parametric oscillator (OPO).[47,54] This can be an OPO based on random quasi-phase-matching, with the benefit of displaying several resonances over a few hundred nanometers.

The full potential of assembled noncentrosymmetric photonic materials is still underexplored. Indeed, the flexibility of the fabrication combining nanocrystals in suspension, where both refractive indices can be modified, with bottom-up methods is a real asset to developing structured devices with multifuntionality responses. For example, nanocrystal photonic assemblies are promising candidates to obtain 3D nonlinear

https://doi.org/10.1021/acsphotonics.2c00081
ACS Photonics 2022, 9, 2193−2203

photonic crystals that are extraordinarily challenging to fabricate with top-down approaches.[51] So far, 3D nonlinear photonic crystals over small surface areas with few layers have been demonstrated. In the future, other effects such as sum-frequency generation or optical parametric processes within these crystals can be studied. Also, solitons can be realized.[55] Therefore, they can be employed to transport information over long distances without losses. Nonlinear photonic crystals can control by design, both the dispersion level and optical nonlinearity, and as a result, enable the soliton propagation.[55] Other applications of 3D nonlinear photonic crystals composed of nanocrystal assemblies are ultranarrow bandwidth quantum light sources based on SPDC, high-frequency acoustic wave generation, and high-density data storage due to the possibility of creating multiplexed nonlinear holograms,[56] as described by Zhang et al.[51] Another interesting field is Anderson localization that can be explored with disordered 3D photonic crystals and has numerous implications in quantum optics.[57,58]

Finally, $\chi^{(2)}$ materials are the key components of quantum sources based on parametric processes.[59−61] Since we have shown that disordered $\chi^{(2)}$ assemblies generate efficient or controllable second harmonic waves, it should be possible to exploit them to produce tailored spontaneous parametric down-conversion (SPDC). In fact, a promising future direction is to use $\chi^{(2)}$ assemblies to generate SPDC and to develop simple and phase-matching free quantum sources based on disordered nanocrystals. Furthermore, both $LiNbO_3$ and $BaTiO_3$ in their bulk form are piezoelectric, pyroelectric, and photoelastic, which are still unexplored at those small scales. Combined with the optical properties of noncentrosymmetric nanocrystal assemblies, they can form a novel family of nanosized optical sensors and transducers.

AUTHOR INFORMATION

Corresponding Author

Artemios Karvounis − *ETH Zurich, Optical Nanomaterial Group, Institute for Quantum Electronics, Department of Physics, 8093 Zurich, Switzerland;* orcid.org/0000-0002-0045-7639; Email: karvounis@phys.ethz.ch

Authors

Viola Valentina Vogler-Neuling − *ETH Zurich, Optical Nanomaterial Group, Institute for Quantum Electronics, Department of Physics, 8093 Zurich, Switzerland*

Andrea Morandi − *ETH Zurich, Optical Nanomaterial Group, Institute for Quantum Electronics, Department of Physics, 8093 Zurich, Switzerland;* orcid.org/0000-0001-8199-1536

Helena Weigand − *ETH Zurich, Optical Nanomaterial Group, Institute for Quantum Electronics, Department of Physics, 8093 Zurich, Switzerland;* orcid.org/0000-0003-0558-5899

Eric Dénervaud − *ETH Zurich, Optical Nanomaterial Group, Institute for Quantum Electronics, Department of Physics, 8093 Zurich, Switzerland*

Rachel Grange − *ETH Zurich, Optical Nanomaterial Group, Institute for Quantum Electronics, Department of Physics, 8093 Zurich, Switzerland;* orcid.org/0000-0001-7469-9756

Complete contact information is available at: https://pubs.acs.org/10.1021/acsphotonics.2c00081

Author Contributions

†These authors contributed equally to this work.

Funding

This work was supported by the Swiss National Science Foundation Grants 179099 and 150609, the European Union's Horizon 2020 research and innovation program from the European Research Council under the Grant Agreement Nos. 714837 (Chi2-nano-oxides) and 862346 (PolarNon). A.K. acknowledges financial support from the European Union's research and innovation Programme under the Marie Skłodowska-Curie Grant Agreement No. 801459, FP-RESO-MUS and the Swiss National Science Foundation through the NCCR MUST. H.W. acknowledges financial support from the Physics Department at ETH Zurich.

Notes

The authors declare no competing financial interest.

ACKNOWLEDGMENTS

The authors thank Ülle-Linda Talts for conducting the atomic force measurement of the thin film in Figure 2c.

REFERENCES

(1) Garmire, E. Nonlinear Optics in Daily Life. *Opt. Express* **2013**, *21*, 30532.

(2) Karvounis, A.; Timpu, F.; Vogler-Neuling, V. V.; Savo, R.; Grange, R. Barium Titanate Nanostructures and Thin Films for Photonics. *Adv. Opt. Mater.* **2020**, *8*, 2001249.

(3) Rabiei, P.; Gunter, P. Optical and electro-optical properties of submicrometer lithium niobate slab waveguides prepared by crystal ion slicing and wafer bonding. *Appl. Phys. Lett.* **2004**, *85*, 4603−4605.

(4) Ulliac, G.; Calero, V.; Ndao, A.; Baida, F. I.; Bernal, M. P. Argon Plasma Inductively Coupled Plasma Reactive Ion Etching study for Smooth Sidewall Thin Film Lithium Niobate Waveguide Application. *Opt. Materials* **2016**, *53*, 1−5.

(5) Le Xuan, L.; Brasselet, S.; Treussart, F.; Roch, J. F.; Marquier, F.; Chauvat, D.; Perruchas, S.; Tard, C.; Gacoin, T. Balanced homodyne detection of second-harmonic generation from isolated subwavelength emitters. *Appl. Phys. Lett.* **2006**, *89*, 121118.

(6) He, G. S.; Tan, L. S.; Zheng, Q.; Prasad, P. N. Multiphoton absorbing materials: Molecular designs, characterizations, and applications. *Chem. Rev.* **2008**, *108*, 1245−1330.

(7) Hsieh, C.-L.; Pu, Y.; Grange, R.; Laporte, G.; Psaltis, D. Imaging through turbid layers by scanning the phase conjugated second harmonic radiation from a nanoparticle. *Opt. Express* **2010**, *18*, 20723−20731.

(8) Bonacina, L.; Brevet, P. F.; Finazzi, M.; Celebrano, M. Harmonic generation at the nanoscale. *J. Appl. Phys.* **2020**, *127*, 230901.

(9) Pu, Y.; Grange, R.; Hsieh, C. L.; Psaltis, D. Nonlinear optical properties of core-shell nanocavities for enhanced second-harmonic generation. *Phys. Rev. Lett.* **2010**, *104*, 207402.

(10) Timpu, F.; Sendra, J.; Renaut, C.; Lang, L.; Timofeeva, M.; Buscaglia, M. T.; Buscaglia, V.; Grange, R. Lithium Niobate Nanocubes as Linear and Nonlinear Ultraviolet Mie Resonators. *ACS Photonics* **2019**, *6*, 545−552.

(11) Knabe, B.; Buse, K.; Assenmacher, W.; Mader, W. Spontaneous polarization in ultrasmall lithium niobate nanocrystals revealed by second harmonic generation. *Phys. Rev. B* **2012**, *86*, 195428.

(12) Kim, E.; Steinbrück, A.; Buscaglia, M. T.; Buscaglia, V.; Pertsch, T.; Grange, R. Second-harmonic generation of single $BaTiO_3$ nanoparticles down to 22 nm diameter. *ACS Nano* **2013**, *7*, 5343−5349.

(13) Rendón-Barraza, C.; Timpu, F.; Grange, R.; Brasselet, S. Crystalline heterogeneity in single ferroelectric nanocrystals revealed by polarized nonlinear microscopy. *Sci. Rep.* **2019**, *9*, 1670.

(14) Shiratori, Y.; Pithan, C.; Dornseiffer, J.; Waser, R. Raman scattering studies on nanocrystalline $BaTiO_3$ Part II - Consolidated polycrystalline ceramics. *J. Raman Spectrosc.* **2007**, *38*, 1300−1306.
(15) Sutherland, R. L.; Mclean, D. G.; Kirkpatrick, S. *Handbook of Nonlinear Optics*, 2nd ed.; Marcel Dekker, Inc.: New York, 2003.
(16) Zgonik, M.; Bernasconi, P.; Duelli, M.; Schlesser, R.; Gunter, P.; Garrett, M. H.; Rytz, D.; Zhu, Y.; Wu, X. Dielectric, elastic, piezoelectric, electro-optic, and elasto-optic tensors of $BaTiO_3$ crystals. *Phys. Rev. B* **1994**, *50*, 5941.
(17) Zhu, D. I.; Shao, L.; Yu, M.; Cheng, R.; Desiatov, B.; Xin, C. J.; Hu, Y.; Holzgrafe, J.; Ghosh, S.; Shams-Ansari, A.; Puma, E.; Sinclair, N.; Reimer, C.; Zhang, M.; Lončar, M. Integrated photonics on thin-film lithium niobate. *Adv. Opt. Photon.* **2021**, *13*, 242−352.
(18) Dicken, M. J.; Sweatlock, L. A.; Pacifici, D.; Lezec, H. J.; Bhattacharya, K.; Atwater, H. A. Electrooptic modulation in thin film barium titanate plasmonic interferometers. *Nano Lett.* **2008**, *8*, 4048−4052.
(19) Kormondy, K. J.; Popoff, Y.; Sousa, M.; Eltes, F.; Caimi, D.; Rossell, M. D.; Fiebig, M.; Hoffmann, P.; Marchiori, C.; Reinke, M.; Trassin, M.; Demkov, A. A.; Fompeyrine, J.; Abel, S. Microstructure and ferroelectricity of $BaTiO_3$ thin films on Si for integrated photonics. *Nanotechnology* **2017**, *28*, 075706.
(20) Vogler-Neuling, V. V.; Savo, R.; Pohl, D.; Hendricks, N. R.; Lang, L.; Timofeeva, M.; Schneider, B.; Richter, F. U.; Timpu, F.; Monneret, S.; Starsich, F.; Grange, R. Solution-Processed Barium Titanate Nonlinear Woodpile Photonic Structures with Large Surface Areas. *Phys. Status Solidi B* **2020**, *257*, 1900755.
(21) Karvounis, A.; Vogler-Neuling, V. V.; Richter, F. U.; Dénervaud, E.; Timofeeva, M.; Grange, R. Electro-Optic Metasurfaces Based on Barium Titanate Nanoparticle Films. *Adv. Opt. Mater.* **2020**, *8*, 2000623.
(22) Erdem, D.; Shi, Y.; Heiligtag, F. J.; Kandemir, A. C.; Tervoort, E.; Rupp, J. L.; Niederberger, M. Liquid-phase deposition of ferroelectrically switchable nanoparticle-based $BaTiO_3$ films of macroscopically controlled thickness. *J. Mater. Chem. C* **2015**, *3*, 9833−9841.
(23) Ulrich, R.; Torge, R. Measurement of Thin Film Parameters with a Prism Coupler. *Appl. Opt.* **1973**, *12*, 2901−2908.
(24) Abel, S.; Stöferle, T.; Marchiori, C.; Rossel, C.; Rossell, M. D.; Erni, R.; Caimi, D.; Sousa, M.; Chelnokov, A.; Offrein, B. J.; Fompeyrine, J. A strong electro-optically active lead-free ferroelectric integrated on silicon. *Nat. Commun.* **2013**, *4*, 1671.
(25) Xiong, C.; Pernice, W. H.; Ngai, J. H.; Reiner, J. W.; Kumah, D.; Walker, F. J.; Ahn, C. H.; Tang, H. X. Active silicon integrated nanophotonics: Ferroelectric $BaTiO_3$ devices. *Nano Lett.* **2014**, *14*, 1419−1425.
(26) Edmondson, B. I.; Kwon, S.; Lam, C. H.; Ortmann, J. E.; Demkov, A. A.; Kim, M. J.; Ekerdt, J. G. Epitaxial, electro-optically active barium titanate thin films on silicon by chemical solution deposition. *J. Am. Ceram. Soc.* **2020**, *103*, 1209−1218.
(27) Weis, R. S.; Gaylord, T. K. Lithium niobate: Summary of physical properties and crystal structure. *Appl. Phys. A: Mater. Sci. Process.* **1985**, *37*, 191−203.
(28) Zali, N. M.; Mahmood, C. S.; Mohamad, S. M.; Foo, C. T.; Murshidi, J. A. X-ray diffraction study of crystalline barium titanate ceramics. *AIP Conf. Proc.* **2013**, *1584*, 160−163.
(29) Timofeeva, M.; Bouravleuv, A.; Cirlin, G.; Shtrom, I.; Soshnikov, I.; Reig Escalé, M.; Sergeyev, A.; Grange, R. Polar Second-Harmonic Imaging to Resolve Pure and Mixed Crystal Phases along GaAs Nanowires. *Nano Lett.* **2016**, *16*, 6290−6297.
(30) Tangwiwat, S.; Milne, S. J. Barium titanate sols prepared by a diol-based sol-gel route. *J. Non-Cryst. Solids* **2005**, *351*, 976−980.
(31) Cao, Y.; et al. A Barium Titanate-on-Oxide Insulator Optoelectronics Platform. *Adv. Mater.* **2021**, *33*, 2101128.
(32) Lu, H.; Sadani, B.; Ulliac, G.; Courjal, N.; Guyot, C.; Merolla, J.-M.; Collet, M.; Baida, F. I.; Bernal, M.-P. 6-micron interaction length electro-optic modulation based on lithium niobate photonic crystal cavity. *Opt. Express* **2012**, *20*, 20884−20893.
(33) Kleinman, D. A. Nonlinear Dielectric Polarization in Optical Media. *Phys. Rev.* **1962**, *126*, 1977−1979.
(34) Pohl, D.; Reig Escalé, M.; Madi, M.; Kaufmann, F.; Brotzer, P.; Sergeyev, A.; Guldimann, B.; Giaccari, P.; Alberti, E.; Meier, U.; Grange, R. An integrated broadband spectrometer on thin-film lithium niobate. *Nat. Photonics* **2020**, *14*, 24−29.
(35) Weigand, H.; Vogler-Neuling, V. V.; Escalé, M. R.; Pohl, D.; Richter, F. U.; Karvounis, A.; Timpu, F.; Grange, R. Enhanced Electro-Optic Modulation in Resonant Metasurfaces of Lithium Niobate. *ACS Photonics* **2021**, *8*, 3004−3009.
(36) Messner, A.; Eltes, F.; Ma, P.; Abel, S.; Baeuerle, B.; Josten, A.; Heni, W.; Caimi, D.; Fompeyrine, J.; Leuthold, J. Plasmonic ferroelectric modulators. *J. Lightwave Technol.* **2019**, *37*, 281−290.
(37) Karvounis, A.; Vogler-Neuling, V. V.; Grange, R. 95 MHz Bandwidth Electro-Optic Metasurfaces based on Barium Titanate Nanocrystals. *Conference on Lasers and Electro-Optics (CLEO) 2021*, 2021; pp 1−2.
(38) Kauranen, M.; Zayats, A. V. Nonlinear plasmonics. *Nat. Photonics* **2012**, *6*, 737−748.
(39) MacDonald, K.; Sámson, Z.; Stockman, M.; Zheludev, N. Ultrafast active plasmonics. *Nat. Photonics* **2009**, *3*, 55−58.
(40) Melikyan, A.; et al. High-speed plasmonic phase modulators. *Nat. Photonics* **2014**, *8*, 229−233.
(41) Nordlander, J.; Eltes, F.; Reynaud, M.; Nürnberg, J.; De Luca, G.; Caimi, D.; Demkov, A. A.; Abel, S.; Fiebig, M.; Fompeyrine, J.; Trassin, M. Ferroelectric domain architecture and poling of $BaTiO_3$ on Si. *Phys. Rev. Materials* **2020**, *4*, 034406.
(42) Visser, D.; Chen, D. Y.; Désières, Y.; Ravishankar, A. P.; Anand, S. Embossed Mie resonator arrays composed of compacted TiO_2 nanoparticles for broadband anti-reflection in solar cells. *Sci. Rep.* **2020**, *10*, 12527.
(43) Richter, F.; Vogler-Neuling, V.; Flavia, T.; Karvounis, A.; Pohl, D.; Weigand, H.; Escale, M.-R.; Grange, R. Electrically Tunable Optical Metasurfaces with Barium Titanate Nanoparticles. *in Conference on Lasers and Electro-Optics OSA Technical Digest*; Optica Publishing Group, 2020; paper FM3B.7.
(44) Timpu, F.; Reig Escalé, M.; Timofeeva, M.; Strkalj, N.; Trassin, M.; Fiebig, M.; Grange, R. Enhanced Nonlinear Yield from Barium Titanate Metasurface Down to the Near Ultraviolet. *Adv. Opt. Mater.* **2019**, *7*, 1900936.
(45) Baudrier-Raybaut, M.; Haıdar, R.; Kupecek, P.; Lemasson, P.; Rosencher, E. Random quasi-phase-matching in bulk polycrystalline isotropic nonlinear materials. *Nature* **2004**, *432*, 374−376.
(46) Müller, J. S.; Morandi, A.; Grange, R.; Savo, R. Modeling of Random Quasi-Phase-Matching in Birefringent Disordered Media. *Phys. Rev. Appl.* **2021**, *15*, 064070.
(47) Ru, Q.; Lee, N.; Chen, X.; Zhong, K.; Tsoy, G.; Mirov, M.; Vasilyev, S.; Mirov, S. B.; Vodopyanov, K. L. Optical parametric oscillation in random polycrystalline medium. *Optica* **2017**, *4*, 617−618.
(48) Qiao, Y.; Ye, F.; Zheng, Y.; Chen, X. Cavity-enhanced second-harmonic generation in strongly scattering nonlinear media. *Phys. Rev. A* **2019**, *99*, 043844.
(49) Savo, R.; Morandi, A.; Müller, J. S.; Kaufmann, F.; Timpu, F.; Reig Escalé, M.; Zanini, M.; Isa, L.; Grange, R. Broadband Mie driven random quasi-phase-matching. *Nat. Photonics* **2020**, *14*, 740−747.
(50) Keren-Zur, S.; Ellenbogen, T. A new dimension for nonlinear photonic crystals. *Nat. Photonics* **2018**, *12*, 575−577.
(51) Zhang, Y.; Sheng, Y.; Zhu, S.; Xiao, M.; Krolikowski, W. Nonlinear photonic crystals: from 2D to 3D. *Optica* **2021**, *8*, 372.
(52) Melikyan, A.; et al. High-speed plasmonic phase modulators. *Nat. Photonics* **2014**, *8*, 229.
(53) Ma, H.; Jen, A.-Y.; Dalton, L. Polymer-Based Optical Waveguides: Materials, Processing, and Devices. *Adv. Mater.* **2002**, *14*, 1339.
(54) Kawamori, T.; Ru, Q.; Vodopyanov, K. L. Comprehensive Model for Randomly Phase-Matched Frequency Conversion in Zinc-Blende Polycrystals and Experimental Results for ZnSe. *Phys. Rev. Appl.* **2019**, *11*, 054015.

https://doi.org/10.1021/acsphotonics.2c00081
ACS Photonics 2022, 9, 2193−2203

(55) Kivshar, Y. S.; Agrawal, G. P. In *Solitons in photonic crystals*; Kivshar, Y. S., Agrawal, G. P., Eds.; Academic Press: Burlington, 2003; Chapter 12, pp 425−446.
(56) Arie, A. Storing and retrieving multiple images in 3D nonlinear photonic crystals. *Light Sci. Appl.* **2021**, *10*, 202.
(57) John, S. Localization of Light. *Phys. Today* **1991**, *44*, 32−40.
(58) Vasco, J. P.; Hughes, S. Anderson Localization in Disordered LN Photonic Crystal Slab Cavities. *ACS Photonics* **2018**, *5*, 1262−1272.
(59) Thew, R. T.; Tanzilli, S.; Tittel, W.; Zbinden, H.; Gisin, N. Experimental investigation of the robustness of partially entangled qubits over 11 km. *Phys. Rev. A* **2002**, *66*, 5.
(60) Couteau, C. Spontaneous parametric down-conversion. *Contemp. Phys.* **2018**, *59*, 291.
(61) Tanzilli, S.; De Riedmatten, H.; Tittel, W.; Zbinden, H.; Baldi, P.; De Micheli, M.; Ostrowsky, D. B.; Gisin, N. Highly efficient photon-pair source using periodically poled lithium niobate waveguide. *Electron. Lett.* **2001**, *37*, 26−28.

https://doi.org/10.1021/acsphotonics.2c00081
ACS Photonics 2022, 9, 2193−2203